PHYSICAL REVIEW B VOLUME 60, NUMBER 7 15 AUGUST 1999-I

Nonlinear dynamic instability in brittle fracture of GaAs

K. Sauthoff, M. Wenderoth,* A. J. Heinrich,[†] M. A. Rosentreter,[‡] K. J. Engel, T. C. G. Reusch, and R. G. Ulbrich
4. Physikalisches Institut, Universität Göttingen, Bunsenstraße 13, D-37073 Göttingen, Germany

(Received 23 February 1999)

The process of brittle fracture in gallium arsenide was investigated to clarify the relation between the dynamics of crack propagation and the observed structure on the fracture surface with time-sensitive and structure-sensitive methods. Within the full range of length scales, i.e., spanning eight orders of magnitude from angstrom units to centimeters, the fracture surface was characterized with a manifold of structure-sensitive methods comprising optical microscopy, profilometry, atomic force microscopy, and scanning tunneling microscopy. We found that it is possible to predict the *local* atomic-scale microstructure of a fracture surface from the knowledge of the *global* macrostructure. The investigation of the fracture kinetics showed that the crack propagation process is characterized by three distinct velocity ranges. The present experimental results on structure and kinetics are consistently interpreted within the framework of a nonlinear dynamic instability in crack propagation. [S0163-1829(99)07131-3]

I. INTRODUCTION

Science and technology have been dealing with the omnipresent phenomenon of (brittle) fracture because of its scientific and—above all—economic importance. For a thorough understanding of the process of brittle fracture, one has to consider various aspects. (i) A large range of length scales of many orders of magnitude has to be included in the structural examination: The crack starts by breaking bonds between individual atoms and ends with global rupturing a sample of macroscopic dimensions. (ii) The sensitive dependence of the fracture process on the macroscopic and microscopic initial and/or boundary conditions has to be taken into account, which means together with the large number of degrees of freedom that the fracture process as a nonlinear many-body phenomenon is generally unpredictable. (iii) The time evolution of the crack propagation process has to be related to the structure of the fracture surface in real space.

In the 1920s, Griffith developed a macroscopic model for fracture[1] based on continuum mechanics.[2] In this first model, he already proposed the Rayleigh wave velocity v_{Rayleigh} to be a theoretical upper limit for the crack propagation velocity, and independent of other sample specifications. New experimental results[3,4] and molecular-dynamics (MD) simulations[4–6] obtained during the past ten years indicated a much smaller but nevertheless general asymptotic velocity (about 60% of the Rayleigh velocity). In addition, they found a sharp transition from a smoothly rising velocity to an oscillating velocity during the fracture process depending on the boundary conditions. This transition was characterized by a second critical velocity v_C which was determined to be 35% of the Rayleigh wave velocity. These results led to microscopic models on the atomic scale[3–5] and to the concept of a nonlinear dynamic instability determining the fracture process, first proposed by Fineberg *et al.*[3] This concept is based on energetic arguments: The fracture energy which scales with the crack length L, and the kinetic energy which scales with v^2L^2 (with v the crack propagation velocity), are converted into free surface energy during the crack process.[7] The shape of the fracture surface profile depends on the amount of converted energy: Smooth surfaces have a smaller net surface area than rough surfaces, i.e., the total surface energy of smooth surfaces is smaller than that of rough ones. These results clearly indicate a general relation between structure and crack dynamics. Moreover, the fact that, e.g., a general roughness exponent for fracture surfaces independent of sample materials and sample sizes exists indicates that brittle fracture has an underlying and somewhat universal fracture mechanism.[8]

Experimentally both aspects—structure and kinetics—were commonly investigated on a *macroscopic* scale. Progress in high-resolution microscopy in recent years—scanning electron microscopy (SEM), scanning tunneling microscopy (STM), and atomic force microscopy (AFM)—allowed observations on small length scales down to the atomic level. First experimental studies on the *atomic* structure of the fracture surface[9] showed that the observed morphologies cannot be explained assuming thermodynamic equilibrium of the surface structure even on the atomic scale, i.e., neither the crack propagation process nor the resulting structure can be described in terms of thermodynamic equilibrium.

In this paper we present the combined study of brittle fracture on the *nanometer* scale together with the investigation of the *macrostructure* of the fracture surface and the dynamics of crack propagation. The comparison of our structural and time-resolved experimental data provides evidence that on all scales from atomic dimensions up to sample dimensions, the mutual interaction of structure and dynamics is caused by one and the same nonlinear dynamic instability.

II. EXPERIMENT

A. Sample preparation

We performed our experiments on the covalent system GaAs, which is a nearly ideal model system due to its extreme brittleness. Although other materials may be more relevant for application, they are not as suitable for studying pure brittle fracture as GaAs because they show neither pure brittle nor pure ductile behavior, but rather a mixture of both.

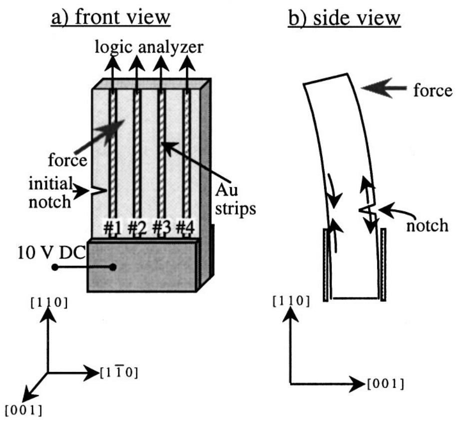

FIG. 1. Experimental cleavage setup (schematic). (a) Front view of the prepared sample, held with jaws in a minivice. (Note that the Au strips are evaporated both on the front and on the back side. The sample is prepared for the fracture kinetics measurements with electric connections; it can be transferred in the STM vacuum chamber only without them.) (b) Bending geometry of the loaded sample (the front part is stressed in tension, the back part is compressed; the crystallographic directions are indicated).

Two different types of material were used: Since the STM investigations require a conductive sample, doped material was used, i.e., $10^{18}\,\mathrm{cm}^{-3}$ *p*-type (Zn) and $10^{18}\,\mathrm{cm}^{-3}$ *n*-type (Si) GaAs. For the crack velocity measurements, metal strips perpendicular to the crack direction were deposited by evaporation, with four strips on the front and four strips on the back of the sample (see Fig. 1) to serve as local probes for the crack propagation. To avoid short-circuiting between the strips via the sample material, semi-insulating GaAs was used in these experiments.

After cutting the sample from a commercially available GaAs [001] wafer,[10] Au or Au/Ge strips were deposited and annealed to form Ohmic contacts on the crystal surface required for the STM measurements. The sample was mounted in a minivice suitable for UHV and notched at one edge (see Fig. 1) to fix the position of the fracture plane. The fracture process was initiated by applying a slowly increasing force to the upper part of the sample according to Fig. 1. Considering the asymmetric stress application and the nonsquare cross section, the stress state is approximately a mode I tension (see Sec. IV). The orientation of the fracture surfaces is the same in all figures (horizontal [001] direction, vertical $[1\bar{1}0]$ direction).

B. Kinetic measurements—setup

We measured the kinetics of the crack propagation process to estimate the range of the relevant crack velocities using samples as shown in Fig. 1(a). The lower parts of the deposited gold strips were connected to a 10 V dc voltage source via the holding device; the upper part of each strip was linked individually to a logic analyzer (HP 1630A) which was used as a digital eight-channel oscilloscope. Each strip had a width of 200 μm, with a spacing of 1 mm between two strips. When the sample fractured perpendicularly to the strips, the strips were ruptured one after the other according to the course of the fracture. The logic analyzer recorded the ruptures as changes in the measured signals from one to zero as a function of time. In the following we will refer to the term ''signal'' as the time when a certain Au strip breaks; $t=0$ is set to the rupture of the first strip. The time resolution was better than 200 ns.

C. Structure analysis—setup

The fracture surfaces were characterized in detail using various methods to cover the whole range of relevant length scales. Optical microscopy/profilometry, AFM, and STM were used for structure analysis on the microscopic (1 mm to 0.5 μm), mesoscopic (in the present experiments in the range of 100 μm to 100 nm), and microscopic (1 μm to 0.1 nm) scale, respectively.

To obtain information on the width and the height of the structures visible in the micrometer range, the fracture surfaces were investigated by optical microscopy and by profilometry. The optical characterization (using an Olympus BH-2 UMA) was performed outside the UHV with a lateral resolution of about 2 μm (see Fig. 3). The profilometer measurements were carried out with a DEKATEST^{3}ST profilometer. The resolution limits were 1 nm for vertical structures and 0.5 μm for lateral structures. In Fig. 4 a set of profilometer results is shown with height data referring to the (110) surface plane. In the left inset the scan positions and directions are given. The scan lengths were 500 μm.

The mesoscopic scale structures were investigated by atomic force microscopy (AFM), using an AFM (DI Multimode Nanoscope™) to detect height differences as small as monatomic steps in large area scans (up to $100\times100\,\mu\mathrm{m}^2$; see Fig. 5).[11]

To characterize the sample surfaces on the microscopic scale, a custom-made UHV cross-sectional scanning tunneling microscope (XSTM) (Ref. 12) with an *in situ* tip and sample exchange was used. For the STM measurements, the samples were cleaved inside the vacuum chamber to avoid contaminations of the investigated surfaces. The XSTM setup allowed the positioning of the tip on the fracture surface within a range of $6\times6\,\mathrm{mm}^2$ with a maximum accuracy of 10 nm. The tip movements by means of a slip-stick mechanism were controlled by a custom-made optical setup. These features made it possible to approach the STM tip (etched tungsten wire) to preselected sites of the sample surface. The STM was thus used as a profilometer with atomic resolution. For the geometry of the cleavage process, see Fig. 1. The maximum scan area was $2\times2\,\mu\mathrm{m}^2$; typical scan ranges were some ten nanometers up to a micrometer (Fig. 6).

III. RESULTS

Due to the large amount of kinetic and structural experimental results determined with multiple methods, we first present an overview of the facts in this section, which will be discussed in detail in the following section.

A. Kinetics

The experimental results showed that the measured duration of the fracture process was $t_{\mathrm{meas}}=14,...,20\,\mu$s for a fracture length of $s_{\mathrm{tot}}=3.6$ mm [t_{meas} is the time between the first and the last measured signal; s_{tot} is the direct distance be-

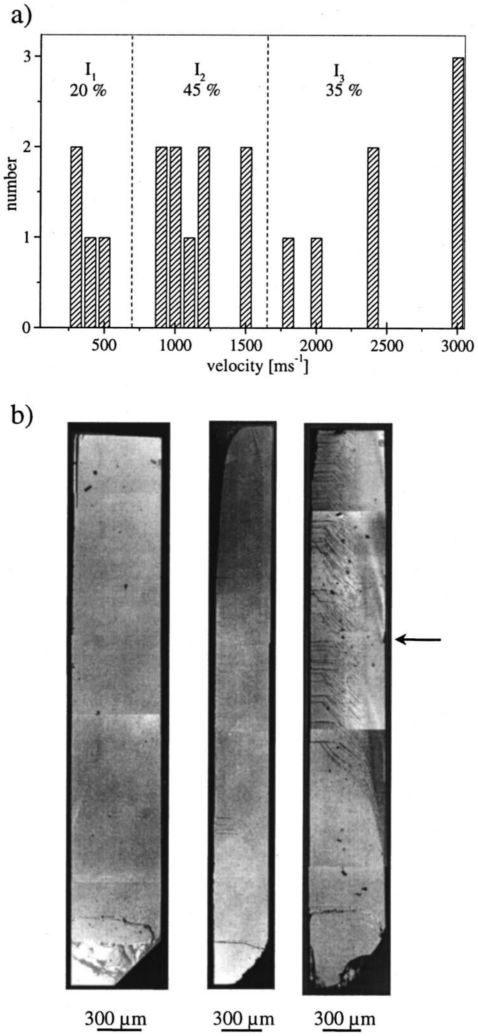

FIG. 2. Time-resolved measurements. (a) Histogram of the measured crack velocities. (b) Left: fracture surface with nearly no visible structures (average velocities within interval I_A); center: with moderate visible structures (average velocities within interval I_B); and right: fracture surface with strongly visible structures (average velocities within interval I_C).

tween the first and the last (eighth) strip]. The four strips on the front will be referred to as nos. 1 to 4 (see Fig. 1). We observed (i) that the signals of strips nos. 1 to 4 appeared according to the order of the strips on the sample surface and (ii) that there was always a time lag in the sequence of the measured signals. After detection of the first group of signals (nos. 1 to 4) a delay of 5 to 8μs is observed until the second group of signals arrived indicating the rupture of the strips on the back.[13]

Based on the data of strips nos. 1 to 4, the average crack velocity was determined via $\langle v \rangle_k = \Delta s/(t_{ik} - t_{i+1,k})$ (with spacing $\Delta s = 1.2\,\mathrm{mm}$ of the left edges of two neighboring strips and time signals $t_{ik}, t_{i+1,k}$ from gold strips i and $i+1$ of sample k). A histogram of the measured velocities is shown in Fig. 2(a).

In order to determine whether the crack propagation velocity is related to the global structure of the fracture surface [Fig. 2(b)], we characterized the surfaces optically. The comparison showed that the values grouped into three intervals. Low velocities (interval $I_A = [0;600\,\mathrm{ms}^{-1}]$) were related to cracks which produced *optically flat* surfaces [referred to as type *A* surfaces; Fig. 2(b), left]. Cracks which propagated with medium average velocities (interval $I_B = [800\,\mathrm{ms}^{-1};1400\,\mathrm{ms}^{-1}]$) produced fracture surfaces with characteristic line patterns [referred to as type *B* surfaces, Fig. 2(b), center]. Based on the local structure of the line patterns, we found that every type *B* surface divided up into six areas, which were found in different distinctness, but in identical order on each of the type *B* surfaces. Each single area showed an individual pattern type—see Figs. 3(a) and 3(b) and the next section. In the following this group of six areas will be referred to as the *characteristic crack pattern* (CCP). Cracks with high propagation velocities (interval $I_C = [1800\,\mathrm{ms}^{-1};3000\,\mathrm{ms}^{-1}]$) produced surfaces showing a sequence of more than one CCP [referred to as type *C* surfaces, Fig. 2(b), right]. 45% of the observed velocities are in I_B, 20% in I_A, and 35% in I_C. These three intervals represent the distinct velocity ranges which characterize the fracture process.

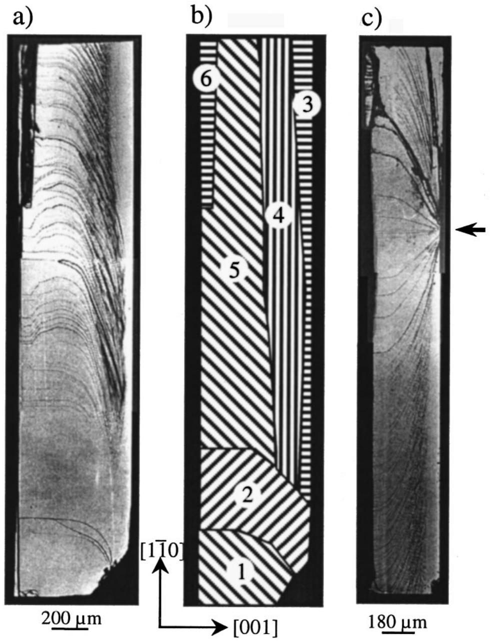

FIG. 3. Optical characterization. (a) Micrograph of a fracture surface (area $2.9\times 0.6\,\mathrm{mm}^2$), type *B*, GaAs sample, initial notch is in the lower right. (b) Schematic representation of the six different areas of the fracture surface. (c) Micrograph of fracture surface (area $2.9\times 0.6\,\mathrm{mm}^2$), type *B* surface, GaAs sample, cleaved without initial notch.

B. Structure analysis

The three types of surfaces *A,B,C* were characterized in more detail over the whole range of relevant length scales. The type *A* surfaces showed a fracture surface that appeared perfectly flat in the optical microscope with weak structures only visible near the initial notch. In AFM and STM measurements, these surfaces were also found to be flat on the atomic scale over the whole fracture surface. Only a few monatomic steps occurred with step densities in the range of 10 $\mu\mathrm{m}^{-1}$ down to 3 $\mu\mathrm{m}^{-1}$.

The subdivision of the CCP on a type *B* surface, i.e., the typical position and size of the areas 1 to 6, is shown in Figs. 3(a) and 3(b). The transition between two areas is continuous, as can be seen in the optical microscope picture [Fig. 3(a)]. The sharp lines of Fig. 3(b) show schematically the borders between the individual areas. Since the line patterns on *both fragments* of each cracked sample were observed as image and mirror image, we conclude that the line patterns were produced during the fracture process and are *not* due to a relaxation process of an initially different surface structure. In addition, we also investigated samples which were cleaved without being notched before—shown in Fig. 3(c). If we take the point marked by an arrow in Fig. 3(c) as the starting point of the fracture process, it can be seen that, in both directions, the CCP was formed. Accordingly, the sequence of CCP's on type *C* surfaces [Fig. 2(b), right part] is explained by the assumption that the fracture process was nucleated at more than one site—see the next section.

The characteristic features of the individual areas of the CCP on the fracture surface are as follows.

Area 1. Area 1 extends near the initial notch over the whole width and over approximately $\frac{1}{8}$ of the length of the fracture surface and shows several rough, high steps. In addition, GaAs fragments from notching were usually found in this area, which made AFM and STM measurements impossible. As is known from the time-resolved measurements, area 1 is formed during the initial stage of the crack propagation.

Area 2. Area 2 also extends over the whole width and borders on area 1 with small, optically visible features between plateaus. The AFM measurements [Fig. 5(a)] showed large, atomically flat plateaus, separated by monatomic steps with average terrace width $\langle b\rangle_2$ (Ref. 14) in the range of 1–5 μm. The monatomic steps form an angle of $\vartheta_2 \approx 45°$ with the $[1\bar{1}0]$ direction. Dislocations were also observed in this area [encircled in Fig. 5(a)]. Probably, they were produced during the crack process. In brittle fracture, dislocations are reported to be asymptotically bound to the crack tip (i.e., dislocations cannot propagate free, they are in most cases consumed by the crack tip) and not asymptotically free (i.e., dislocations can propagate through the whole material)[5] as in ductile materials.

These results indicate that the directions of the microscopic steps are the same as those of the visible lines.

Area 3. Area 3 adjoins area 2 and forms a strip parallel to the $[1\bar{1}0]$ direction; it is positioned directly at the sample edge. On the macroscopic scale no structural features were detected as can be seen in the profilometer measurements (Fig. 4, scan *A*): The sample surface is flat with an angle of inclination of $\langle\varphi\rangle_3 = 0.5(1)°$ to the (110) surface. On the microscopic scale, furrowed structures with mostly monatomic steps were observed, but also higher steps up to ten monolayers were measured [Fig. 6(b)].[15] The average terrace width is $\langle b\rangle_3 = 13(2)$ nm [Fig. 6(b)]. The average angle to the $[1\bar{1}0]$ direction is $\langle\vartheta\rangle_3 = 10°$. Further experimental data (from different samples of type *B*) indicated an average terrace width $\langle b\rangle_3$ between 10 and 25 nm and an average angle $\langle\vartheta\rangle_3$ within the interval 10°–14°.

Area 4. Area 4 adjoins areas 2 and 3 and forms a strip parallel to the $[1\bar{1}0]$ direction with many fine structures visible in the optical microscope. The profilometer measurements show a monotonous step sequence—see profilometer-scan *B* (Fig. 4), the terraces being (110) surfaces. The average inclination angle is $\langle\varphi\rangle_4 = 0.5(1)°$, which is equal to $\langle\varphi\rangle_3$. The average macroscopic terrace width is $\langle b\rangle_4 = 14(1)\,\mu$m and the average step height is $\langle h\rangle_4 = 128(11)$ nm. The wide macroscopic terraces displayed a further monatomic microstructure which was measured by AFM [Fig. 5(b)] and STM [Figs. 6(c) and 6(d)]. The observed microscopic structures became more staircaselike with increasing distance from the transition to area 3 [Fig. 6(c)], i.e., this implies a growing nanoscale roughness. The average microscopic terrace width in the center of area 4 is 10(2) nm [Fig. 6(c)], which is in the same range as in area 3. Triangular structures are observed near the transition to area 5 as can be seen in the micrograph of Fig. 6(d). The direction of the steps changed depending on the distance from the frontal cleavage edge: In the transition region to area 3 they are oriented nearly parallel to the $[1\bar{1}0]$ direction; in the center of area 4 the angle to the $[1\bar{1}0]$ direction is 17°. Near the transition to area 5, $\langle\vartheta\rangle_4$ is in the range 20°–38° [Fig. 6(d)], i.e., the steps which run parallel to the $[1\bar{1}0]$ direction near the sample edge bend to run perpendicular to this direction on approaching the back of the sample. The comparison of macroscopic and microscopic data shows that the direction of the microscopic steps is parallel to the visible lines.

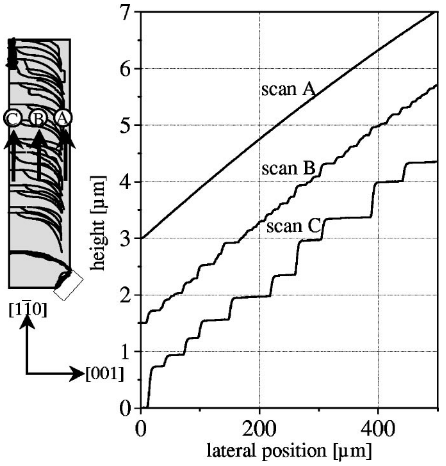

FIG. 4. Profilometer measurements of height as a function of position. The locations and scan directions of scans *A* to *C* are indicated in the left part of the figure. The scan length was 0.5 mm in each scan. The scans are shifted in vertical direction for clarity.

Area 5. Area 5 adjoins area 2 and is positioned at the rear edge of the sample, forming a strip parallel to the $[1\bar{1}0]$ direction. Compared to areas 3 and 4, area 5 has less macroscopic structure which runs nearly perpendicular to the $[1\bar{1}0]$ direction. The average terrace width and step height as determined by profilometry are $\langle b\rangle_5 = 50(5)\,\mu$m and $\langle h\rangle_5 = 350(43)$ nm, respectively, the terraces being (110) surfaces. This indicates that the macroscopic steps are significantly higher than in area 2. The angle of inclination to the (110) surface is 0.5(1)°, which is the same as $\langle\varphi\rangle_3$ and $\langle\varphi\rangle_4$. In contrast to area 4, the (110) terraces showed no microstructure, i.e., atomically flat plateaus were observed by STM.

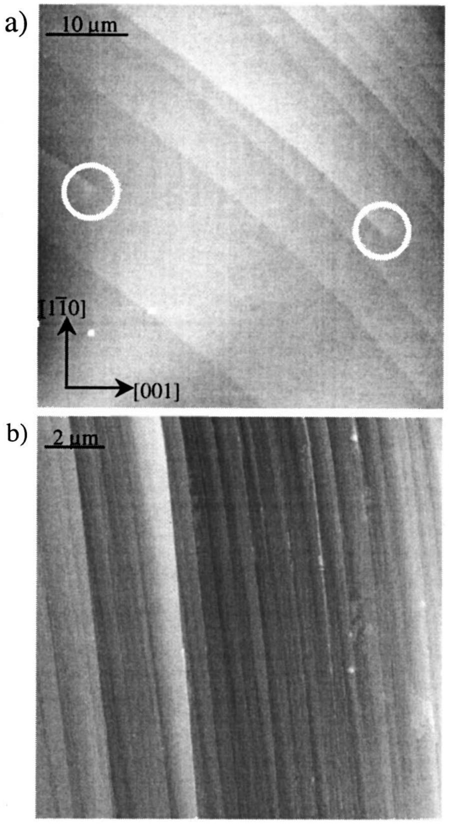

FIG. 5. AFM measurements (Ref. 11). (a) Area 2 with a scan area of (50 μm)^2. Dislocations (encircled) are visible in the center at the left and right edge. The lines indicate monatomic steps. (b) Area 4 with a scan area of (16.6 μm)^2. The crystallographic directions are given in (a) and are the same for both micrographs.

Area 6. Area 6 is in the upper left part of the fracture surface and has very rough features. The rough, high steps made AFM and STM measurements impossible for this area.

In the detailed structural investigations presented in this section, we found that type *A* surfaces are flat on the macroscopic as well as on the nanometer scale, whereas in the different areas of the type *B* CCP the various macrostructures showed atomic substructures with distinct step densities, step heights, and step directions.

IV. DISCUSSION

The investigated samples have a nonsquare cross section (the ratio width to thickness is in the range of 1:5 for STM samples to 1:10 for the kinetic samples). That means that the crack tip in the back part of the sample (area 5) is influenced by the sample edges. This is different from pure mode I loading, which assumes infinitely thick material in front of the crack tip. Nevertheless, the bending geometry as well as the applied stress field guarantee a mode I loading in the front part of the sample (areas 1 to 4).

To analyze our experimental results in the framework of a nonlinear dynamic instability,[3–5] we will first discuss our kinetic data with respect to the relevant fractions of the Rayleigh velocity. Two characteristic velocities have been found in former experiments. The limiting velocity measured, e.g., in experiments investigating poly(methyl methacrylate) (PMMA) was 60% of the Rayleigh wave velocity. A second significant velocity is $v_C = 0.35 v_{\text{Rayleigh}}$. Slower crack propagation velocities ($v < v_C$) result in smooth fracture surfaces, whereas higher crack propagation velocities ($v > v_C$) lead to rough surfaces in the micrometer range.

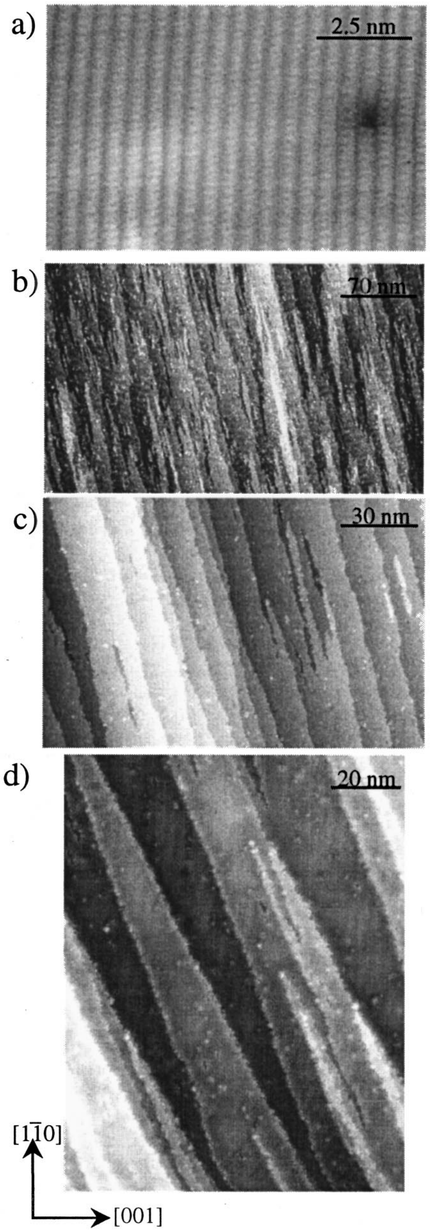

FIG. 6. STM measurements (Ref. 11). (a) Area 2 with a scan area of 12.5×9 nm^2; the *z* scale is 0.4 nm. The monatomic rows along the $[1\bar{1}0]$ direction can be recognized. (b) Area 3 with a scan area of 350×250 nm^2; the *z* scale is 0.8 nm. Furrowed structures are visible. (c) Area 4 with scan area 150×100 nm^2 and *z* scale of 1 nm [parallel monatomic steps (staircaselike structures) are plainly visible]. (d) Area 4 with a scan area of 100×125 nm^2 and *z* scale 1 nm (triangularly shaped structures). The indicated crystallographic directions are the same for all micrographs.

The Rayleigh wave velocities for GaAs are $v_{\text{Rayleigh}(1)} = 2.51 \times 10^3\ \text{ms}^{-1}$ and $v_{\text{Rayleigh}(2)} = 2.97 \times 10^3\ \text{ms}^{-1}$ with the wave vector $\mathbf{k}$ in [110] and [111], respectively.[16] Our measured velocities have a relative systematic error of about 20%. So although GaAs in contrast to PMMA is an anisotropic material, we will use the average Rayleigh velocity $\overline{v}_{\mathrm{Rayleigh}}=2.7\times10^{3}\ \mathrm{ms}^{-1}$ in the following discussion. Assuming the same fraction of the Rayleigh wave velocity as determined from the PMMA experiments[3] and from the computer simulations for the critical velocity values (critical velocity $v_C=0.35v_{\mathrm{Rayleigh}}$ asymptotic velocity $v_{\mathrm{max}}=0.6v_{\mathrm{Rayleigh}}$,[3–5] we obtain the critical velocity $\overline{v}_{C,\mathrm{GaAs}}=0.9\times10^{3}\ \mathrm{ms}^{-1}$ and the asymptotic velocity $\overline{v}_{\mathrm{max,GaAs}}=1.6\times10^{3}\ \mathrm{ms}^{-1}$ as appropriate values for GaAs. These values agree reasonably well with the ranges of the experimental data in Fig. 2(a), which is a clear qualitative agreement between the PMMA measurements and our experimental results with respect to the relevant kinetics.

Furthermore, it is reasonable that some velocities exceed the predicted asymptotic velocity (the values in I_C) if it is taken into account that more than one ''weak point'' as a possible nucleation site for (local) cleavage may exist. The fracture surface of Fig. 2(b), right part, is related to the velocity interval I_C (the arrow marks an artifact in the initial cleavage edge, which is optically flat in type *B* samples). When the crack starts to propagate, sound is emitted from the first crack tip. The sound waves propagate with the bulk sound velocity through the sample transporting energy faster than v_{Rayleigh} and initiating further (local) cleavages at the bent surface of the sample. The artifact in Fig. 2(b) (marked by the arrow) may be a second nucleation site for local cleavage initiated by such acoustic shock waves as discussed above. Some aspects of the influence of sound on the fracture process have been investigated so far: Regarding the relevant energies in the crack propagation, sound effects can be neglected as the sound energy was determined to be only 5% of the total fracture energy in the PMMA experiments.[3] Considering the dynamic point of view, sound plays a more important role in the fracture process because of the strong interference effects of sound waves, which are reflected from the sample edges onto the propagating crack.[17]

From the macroscopic profilometer measurements we conclude that the fracture process produces a planar fracture surface with a uniform angle of inclination over the whole surface within the resolution limits of the profilometer, because the measured steps on different samples along a profilometer line scan were always monotonous. The fracture surface corresponded to the (110) plane only in some cases. Mostly the fracture surface enclosed an angle of $-0.8°\leqslant\langle\varphi\rangle\leqslant0.8°$ from the (110) surface. This is due to the sensible dependence of the fracture process on the boundary conditions: The orientation of the fracture surface is influenced by the way the initial notch had been applied to the sample, which is *not* reproducible on the atomic scale. The comparison of data from single areas of the CCP of different samples showed that the macroscopically measured terrace widths on different surfaces were similar, whereas the step heights varied considerably, which results in different slope angles. Because of this surprising agreement of the terrace widths in the respective areas on different samples, there seems to be a mechanism in the fracture process which produces terraces of nearly equal widths during each particular stage of the fracture process independent of the history of the crack.

The structural investigations showed that ''step bunching'' occurs, e.g., flat steps and narrow terraces near the initial cleavage edge correspond to the high steps and wide terraces in the rear part of the fracture surface, which leads to a uniform angle of inclination over the whole surface. The effect becomes more distinctive when moving the microscopic probe from the front edge (area 3) to the back edge (area 5).

The examinations on the different length scales showed that it *is possible* to conclude from the macroscopic observations to the local microstructure of the fracture surface of type *B* samples. Considering the CCP, the optically flat areas 2 or 3 indicate atomically flat plateaus or furrowed structures, respectively. However, it *is not possible* to distinguish all the types of the fracture surface microstructures from the optically visible features alone. Optically flat regions may comprise atomically flat plateaus or rough monatomic step structures.

Finally, we want to discuss the relation of the structure with respect to the nanometer scale and crack propagation process. We will characterize the fracture surface in areas 2 to 4, which are situated in the mode I loaded part of the sample. Previously published studies on brittle fracture on the macroscopic scale[3–5] claimed that the fracture surfaces change from smooth to rough the faster the crack propagates, i.e., ''smooth'' fracture surfaces are related to $v<v_C$ and ''rough'' ones are related to $v>v_C$. This means in our case that the smooth area 2 is formed in the initial stage of the fracture process as the time-sensitive measurements had shown that the crack started to propagate at the notch. In view of the fact that there was always a time lag between the signals from the front and from the back, we assume that the crack first propagated along the front edge of the sample before it turned and advanced to the back. Accordingly, area 3, which is significantly rougher than area 2 (step densities in area 3 in the range of 70–100 $\mu\mathrm{m}^{-1}$), was formed next after area 2. Area 4 shows macroscopic steps and terraces with a monatomic microstructure, i.e., rougher structures than in area 3 according to the proposed way of crack propagation. In addition to the overall structural results reported in Sec. III A, the nanoscale investigations confirmed that a slowly propagating crack produces smooth surfaces (in terms of the characteristic areas we can say that type *A* surfaces consist of area 1 and a large area 2), whereas fast cracks produce rough surfaces as can be seen in Figs. 2(a) and 2(b) (type *B* and type *C* surfaces) and corroborate previously published studies.[3–5]

If we compare our experimental results with earlier studies on brittle fracture, it is interesting to note that on one hand the theoretical studies brought forward a quite complete description of the brittle fracture process covering the large range of length scales by using multiple methods (atomic molecular dynamics models[4–6] embedded in finite element continuum calculations).[18–20] On the other hand, brittle fracture has experimentally been investigated mainly on the macroscopic scale. Besides the PMMA investigations[3] and measurements of the fracture toughness of GaAs,[21] first results on the dynamic fracture behavior of silicon[22] have been published. Therefore, our results corroborate the experimental side of brittle fracture as they provide the link between the microscopic scale and macroscopic structural and dynamic properties.

V. CONCLUSION

We showed that the dynamic crack propagation in crystalline material is related to the fracture surface topography on all scales. This relation is described in a combined study of kinetic and structural measurements within the concept of dynamic nonlinear instability in crack propagation. In our experiments we used multiple structure-resolving methods to cover the largest possible range of length scales from nanometer dimensions to macroscopic sample dimensions, which allows us to relate the microscopic experimental results to the macroscopic observations.

The Rayleigh wave velocity as well as the bulk sound velocity turned out to be crucial parameters. The maximum fracture propagation velocity is about 60% of the Rayleigh wave velocity. We found a transition from smooth to rough fracture surfaces at a critical velocity of about 35% of the Rayleigh velocity. Additional crack tips ahead of the crack front are most probably initiated by sound, which is emitted during the crack process and propagates with the bulk sound velocity. We observed qualitative and quantitative agreement of the determined critical and asymptotic velocities for GaAs with the PMMA experimental values and the MD calculation values.

Our results corroborate former experimental studies of brittle fracture since we showed that the nanoscale structure is related to the macroscopic structural and dynamic properties. This consistently supports the hypothesis of the existence of a common fracture mechanism which is independent of the used material, its structure, the boundary conditions, and the sample size.

ACKNOWLEDGMENTS

We thank Felix Harbsmeier and Wolfgang Bolse, II. Physikalisches Institut der Universität Göttingen, for the use of the profilometer.

---

*Author to whom correspondence should be addressed. Electronic address: Martin.Wenderoth@physik.uni-goettingen.de

†Present address: IMB Almaden Research Center, D1-232, San Jose, CA 95120-6099.

‡Present address: Klöckner-Moeller GmbH, Abteilung PT, Hein-Moeller-Straße 7-11, 53115 Bonn, Germany.

[1] A. A. Griffith, Philos. Trans. R. Soc. London, Ser. A **221**, 163 (1920).

[2] L. B. Freund, *Dynamic Fracture Mechanics* (Cambridge University Press, Cambridge, MA, 1990).

[3] S. P. Gross, J. Fineberg, M. Marder, W. D. McCormick, and H. L. Swinney, Phys. Rev. Lett. **71**, 3162 (1993); J. Fineberg, S. P. Gross, M. Marder, and H. L. Swinney, *ibid.* **67**, 457 (1991); Phys. Rev. B **45**, 5146 (1992).

[4] M. Marder and J. Fineberg, Phys. Today **49** (9), 24 (1996).

[5] M. Marder and X. Liu, Phys. Rev. Lett. **71**, 2417 (1993); N. J. Wagner, B. L. Holian, and A. F. Voter, Phys. Rev. A **45**, 8457 (1992); F. F. Abraham, D. Brodbeck, R. A. Rafey, and W. E. Rudge, Phys. Rev. Lett. **73**, 272 (1994); B. L. Holian and R. Ravelo, Phys. Rev. B **51**, 11 275 (1995).

[6] F. F. Abraham, D. Schneider, B. Land, D. Lifka, J. Skovira, J. Gerner, and M. Rosenkrantz, J. Mech. Phys. Solids **45**, 1461 (1997).

[7] Definition of the different types of energy as in Ref. 4.

[8] K. J. Måløy, A. Hansen, and E. L. Hinrichsen, Phys. Rev. Lett. **68**, 213 (1992).

[9] M. A. Rosentreter, M. Wenderoth, N. H. Theuerkauf, A. J. Heinrich, M. A. Schneider, and R. G. Ulbrich, Phys. Rev. B **56**, 10 538 (1997); Europhys. Lett. **38**, 675 (1997).

[10] STM samples with dimensions $10\times 2.5\times 0.3\,\mathrm{mm}^3$, samples for the kinetic measurements with dimensions $15\times 5\times 0.3\,\mathrm{mm}^3$.

[11] The code of height information in the following AFM and STM images is as follows: Light structures represent elevation, dark structures represent depression.

[12] The base pressure of the vacuum chamber was 5×10^{-11} mbar; *only the STM measurements* were performed in UHV.

[13] The real fracture time is somewhat larger than t_{meas} because the first signal does not always correspond exactly to the start of the fracture process. The measured signals from the strips of the back appeared randomly due to the different stress distribution in this part of the sample (cracking of the atomic bonds not perpendicular to the fracture surface). That means that the cleavage mechanism is different from that in the front part of the sample and will be treated elsewhere. To measure the fracture time all measured signals (strips 1 to 8) were evaluated; to determine the crack velocity values only the signals from the front (strips 1 to 4) were used.

[14] The indices of the measured quantities indicate the respective area.

[15] For the step height distribution, see Ref. 9; the term ‘‘furrowed’’ is used according to Ref. 9. In contrast, long parallel structures are referred to as ‘‘staircaselike.’’

[16] U. Harten and J. P. Toennies, Europhys. Lett. **4**, 833 (1987).

[17] J. F. Boudet and S. Ciliberto, Phys. Rev. Lett. **80**, 341 (1998).

[18] D. Holland and M. Marder, Phys. Rev. Lett. **80**, 746 (1998).

[19] F. F. Abraham, J. Q. Broughton, N. Bernstein, and E. Kaxiras, Europhys. Lett. **44**, 783 (1998).

[20] B. N. J. Persson, Phys. Rev. Lett. **81**, 3439 (1998).

[21] R. W. Margevicius and P. Gumbsch, Philos. Mag. A **78**, 567 (1998).

[22] T. Cramer, A. Wanner, and P. Gumbsch, Phys. Status Solidi A **164**, R5 (1997).